Chapter I: Introduction

1.1 Transition Metal Oxide: TiO_2

Transition metal oxides are fascinating class of inorganic materials, exhibiting a wide range of crystal structures, properties, and applications. The variety in properties stem from the unique nature of the outer *d*-electrons of the transition metal. Some oxides like $LaNiO_3$, RuO_2, and ReO_3 show metallic behaviour, whereas MnO and $BaTiO_3$ demonstrate insulating properties. These oxides show diverse magnetic properties, like ferromagnetism (e.g., CrO_2, $La_{0.5}Sr_{0.5}MnO_3$), anti-ferromagnetism (e.g., NiO, $LaCrO_3$, $CoTiO_3$) and ferrimagnetism (e.g., Fe_3O_4, $ZnFe_2O_4$, $NiFe_2O_4$). $BaTiO_3$, $KNbO_3$ exhibits ferroelectricity whereas $Gd_2(MoO_4)_3$ show ferroelasticity. They also form the class of Superconducting (e.g., $YBa_2Cu_3O_7$), and Multiferroic (e.g. $TbMnO_3$, $LuFe_2O_4$) materials. These materials offer challenges to physicists as well as material scientists to understand their structural, electronic, magnetic and optical properties for the practical applications. There are some oxides like ZnO, SnO_2, HfO_2, NiO and TiO_2 etc. which belongs to the class of semiconductors. Among these semiconductors, TiO_2 is most promising due to its variety of structures as well as physical properties that make it useful in different fields of application. To begin with, we discuss about the basic structure and properties of TiO_2.

1.1.1 Structure of TiO_2

TiO_2 has three polymorphs namely anatase, rutile and brookite. Among these three phases, anatase is kinetically and rutile is thermodynamically most stable. On heat treatment, anatase phase irreversibly converts to rutile phase. Brookite is basically a metastable phase achieved in high pressure synthesis conditions that also converts to rutile phase on heat treatment.

Among the three phases, rutile is the most stable phase in bulk form. The unit cell of rutile structure is shown as Fig.1.1 (a). Each Ti ion is octahedrally coordinated to six O ions forming a TiO_6 octahedron in a distorted manner, with the apical Ti-O bond length (1.98 Å) being slightly longer than the equatorial Ti-O bond length (1.95 Å). The four equatorial O ions are

coplanar occupying a rectangular arrangement with the long edge (2.954 Å) along the c direction and the short edge (2.53 Å) lying diagonally across the plane defined by the 'a' direction. The chains of TiO_6 octahedra are attached by sharing the edges along the 'c' direction and share vertices in the a-b plane.

The structure of anatase is shown in Fig.1.1(b). The unit cell consists of two units of TiO_2. Each Ti ion is octahedrally coordinated to six O ions. The Ti-O octahedron is not regular and the Ti-O bond distances are similar to those in rutile. The octahedral form zigzag chains along the 'a' and 'b' directions with each octahedron sharing four edges.

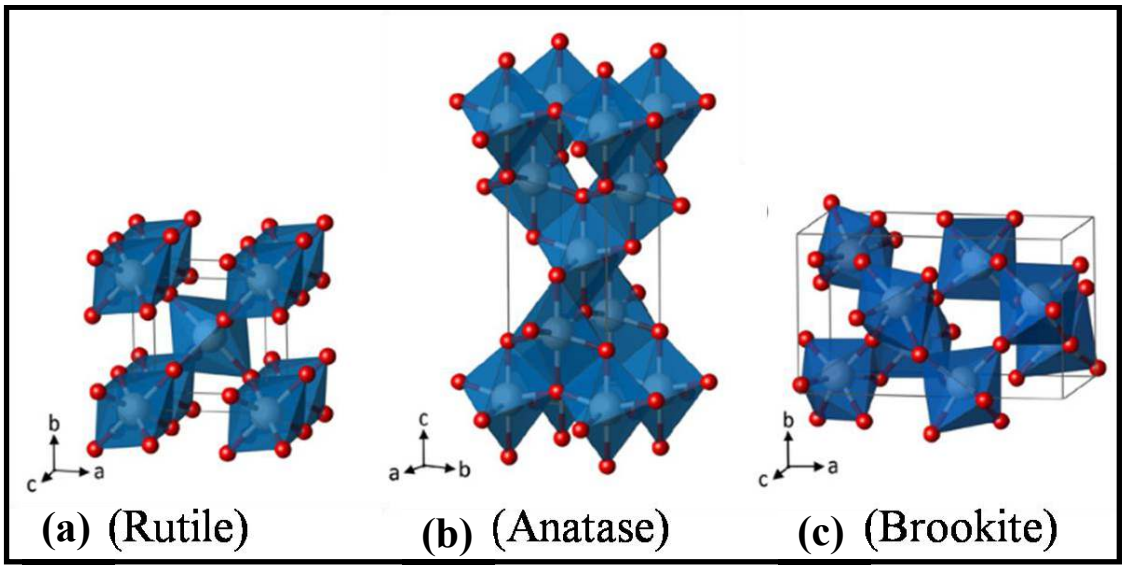

Fig.1.1 TiO_6 polyhedra showing the three polymorphs of TiO_2: rutile (a), anatase (b) and brookite (c). Ti is represented as white and O as red spheres. [After Landmann et al. (2012)]

Besides anatase and rutile, brookite is the less explored phase as it is difficult to synthesize in pure phase form. However, it often appears as a secondary phase along with anantase phase. The basic brookite structure is shown in Fig.1.1(c). In case of brookite, there are six different O-Ti-O bond angles ranging from 77° to 105°. However, rutile and anatase have only two kinds of Ti-O and O-Ti-O bond angles [Muscat et al. (2002)]. The different structural parameters of three crystalline phases are summarized in Table 1.1.

Table 1.1 Structural parameters for the three crystalline phases of TiO_2. [Deryes Cornado et al. (2008)]

	rutile	**anatase**	**brookite**
Crystal Structures	Tetragonal	Tetragonal	Orthorhombic
Lattice Constants (Å)	a = 4.5936 c = 2.9587	a = 3.784 c = 9.515	a = 9.184 b = 5.447 c = 5.145
Space Groups	$P4_2/mnm$	$I4_1/amd$	Pbca
Molecule/Cell	2	4	8
Volume/Molecule	31.2160	34.061	32.17
Density (g/cm^3)	4.13	3.79	3.99
Ti-O bond length (Å)	1.949(4) 1.980(2)	1.937(4) 1.965(2)	1.87-2.04
O-Ti-O Bond angle	81.2^o 90.0^o	77.7^o 92.6^o	$77.0 - 105^o$
Band gap	3.00 (direct)	3.21(indirect)	3.13 (indirect)

1.1.2 Properties of TiO_2

Due to its scientific and practical importance, TiO_2 in rutile phase has been the subject of many experimental and theoretical investigations. Selected reviews in this field are the work of Grant (1959), Goodenough (1971), and Henrichm (1985). The electronic properties of anatase are assumed to be identical as rutile. Forro et al. (1994) have investigated the transport properties and reveal a shallow donor level and high n-type mobility in anatase crystals. Tang et al. (1994) have studied the photoluminescence in the same anatase crystals. Luminescence due to the recombination of self-trapped excitons is observed in anatase crystals, but not in rutile crystals.

In bulk, TiO_2 behaves as a d^0 insulator with empty *d* bands. However, there is a common tendency of having oxygen vacancies in the TiO_2 lattice. These oxygen vacancy related defect states form a shallow donor band below the conduction band makes it an n-type semiconductor [Shinde et al. (2003); Forro et al. (1994)]. In case of highly non-stoichiometric TiO_2, it demonstrates metallic phase at high temperature and shows semiconducting nature at low temperature [Shinde et al. (2003)]. When the non-stoichiometry is sufficiently

high, it favours the formation of magneli phases (Ti_nO_{2n-1}). Due to the basic instinct of having oxygen vacancy, the non-stoichiometry in TiO_2 is often referred as $TiO_{2-\delta}$. Bulk TiO_2 is highly susceptible to oxygen vacancies. These oxygen vacancies further increase when the size is reduced to nanometer scale or thin films grown under oxygen deficient environment. In case of thin films, it is easier to control the oxygen vacancy concentration by controlling the oxygen partial pressure during deposition. It has been reported that rutile is most stable in oxygen deficient condition than that of anatase [Kim et al. (2009)]. Besides vacancy concentration, transport properties also depend on phase of TiO_2 that possess different effective mass of electron carriers as well as mobility. It has been found that anatase phase can easily be switched to metallic system by varying the carrier density than the rutile phase. In view of Mott transition in semiconductors, the critical donor concentration (n_{dc}) for the transition is given by, $n_{dc} \sim (0.25/r_H^*)^3$, where r_H^* is the Bohr radius of hydrogen like donor state. It has been observed that the Bohr radius for anatase phase is much larger than that of rutile phase. As a result, comparatively lower critical donor density is sufficient to induce metallic character in the system [Zhang et al. (2007)]. Hence, we attribute the electrical property of TiO_2 is solely dependent on growth conditions.

In bulk form, TiO_2 is nonmagnetic in nature due to its d^0 configuration. However, Singhal et al. (2011) have reported ferromagnetism in bulk anatase TiO_2 upon hydrogenation. It has been reported both theoretically as well as experimentally that $TiO_{2-\delta}$ demonstrates ferromagnetism when the size is reduced to nanoscale. However, the exact origin of ferromagnetic ordering in these systems is still debated. Similarly, room temperature ferromagnetism has been seen in other inorganic oxides like SnO_2, ZnO, and HfO_2. The possible reasons behind the ferromagnetic ordering in TiO_2 are discussed in Chapter II. As the phase of TiO_2 is an important parameter to decide the physical properties, one needs proper understanding regarding this phase transformation

for possible applications. So it is important to understand the factors that may affect this anatase to rutile phase transformation.

1.1.3 Anatase to Rutile Phase Transformation

The control of anatase to rutile phase transformation is vital for the performance of this material in various applications such as sensors, photocatalysis, pigments and electronics [Vogel et al. (1994)]. Anatase to rutile phase transformation is kinetically defined and solely depends on different parameters like particle size, shape [Yoganarasimhan and Rao (1962)], source effects [Byun et al. (1997)], atmosphere [MacKenzie (1975)] and dopants [Reidy et al. (2006)]. Anatase to rutile transformation is basically a nucleation and growth process [Ding and Liu (1998)]. It is expected that phase transformation could be influenced by defect concentration [Zhang and Banfield (2000)], grain boundary concentration [Ahn et al. (2003)] and particle size [Kumar et al. (1993)] as well. Arroy et al. (2002) have shown the effect of dopants on anatase to rutile phase transformation temperature. Reidy et al. (2006) have reported the enhancement of anatase to rutile phase transformation temperature with an addition of dopants such as Si, Zr and Al, while Co, Mn and V lower the same. Zhang and Banfield (2000) have reported that a critical size mechanism may also be important in the structural phase transition of nanoparticles of TiO_2. The thermodynamics of phase formation in titania is vividly discussed by Zhang and Banfield [Zhang and Banfield (2000)(a)]. Reidy et al. (2006) have examined the critical particle size which is found to be of ~ 45 nm irrespective of dopants. High temperature and pressure involved synthesis techniques yield rutile and brookite phases respectively. We discuss some of the methods to synthesize nanostructured TiO_2 in the following section.

1.2 Synthesis/Deposition of Nanostructured TiO_2

TiO_2 nanoparticles can be synthesised in different phases and morphologies by various techniques like sol-gel, microwave assisted synthesis, micro-emulsion, hydrothermal and combustion techniques. The shape and growth of the nanoparticles can be controlled by using proper capping agents and maintaining suitable growth condition. Detailed method of synthesis of the TiO_2 nanoparticles, nanotubes and nanowires are reported in literature. Some of the popular techniques used for synthesis or deposition of nanostructured TiO_2 are discussed below.

1.2.1 Synthesis of Nanoparticles

Sol-gel Technique

The history of sol-gel processing began in the mid-1800s with Ebelman and Graham's studies on silica gels. Sols are dispersions of colloidal particles in liquid. Colloids are solid particles with diameters of 1-100 nm. A gel is an interconnected, rigid network with pores of submicrometer dimensions and polymeric chains whose average length is greater than a micrometer. [Hench and West (1990)]. A typical self-descriptive pictorial representation of sol-gel process is shown in Fig.1.2.

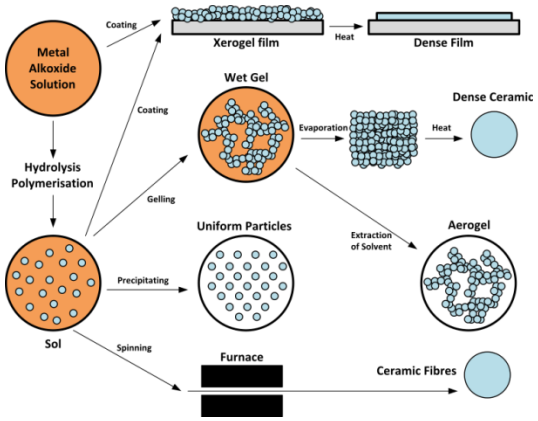

Fig.1.2 Various steps involved in sol-gel process to synthesize nanostructured material.

[from Wikipediahttp://commons.wikimedia.org/wiki/File:Sol Gel_Scheme.svg]

For synthesis of TiO_2 nanoparticles by sol-gel technique, titanium isopropoxide or titanium butoxide are used in place of metal alkoxides. If no gelation inducing reagents (hydrolysis catalysts) are used, the initial hydrolysis of titanium alkoxides results in the formation of titanium hydroxide monomers according to equation (1.1)

$$Ti(OR)_4+4H_2O \rightarrow Ti(OH)_4+4ROH \text{……..……....(1.1)}$$

where R represents the organic chain of the formula- C_xH_{2x+1}

Titanium dioxide having OH terminated surfaces forms and precipitates through the condensation process of hydroxide monomers to form a continuous network of Ti-O bonds. This reaction is described in equation (1.2) that takes place through a nucleation and growth process.

$$Ti(OH)_4 \rightarrow TiO_2 + 2H_2O \text{…….…..(1.2)}$$

Equation (1.1) does not proceed stoichiometrically and in the absence of peptising agents, the rapid formation of partially hydrolysed species occurs as:

$$Ti(OR)_4 + xH_2O \rightarrow Ti(OH)_x(OR)_{4-x} + xROH \text{ ……..(1.3)}$$

This is accompanied by the condensation reaction and resultant precipitation is described by equation (1.4)

$$Ti(OH)_x(OR)_{4-x} + Ti(OR)_4 \rightarrow (OR)_{4-x}Ti\text{-}O_x\text{-}Ti(OR)_{4-x}+xROH \text{ ….(1.4)}$$

In the processing, the Ti to H_2O ratio or the *p*H significantly determines the size, morphology and crystallinity of the final product. Doped and undoped TiO_2 nanoparticles have been synthesised by many groups.

Hydrothermal Technique

In this technique, the reaction takes place in liquid media above the boiling point of water with high pressure. The reaction takes place inside a closed vessel called autoclave. Desired solvents are used to shape the nanoparticles. Treating the reaction mixture for prolonged time enables unique

reactions that may not possible in ambient conditions. TiO_2 nanoparticles with anatase, rutile and brookite phase have been synthesized by this technique [Reyes-Coronado et al. (2008)]. Besides synthesis of nanoparticles, nanowires, and nanotubes faceted single crystals may be grown using this technique [Yang et al. (2008)].

Microwave assisted Technique

Due to high speed, homogeneous selective heating, and easy scalability, the solution-based, microwave-assisted approach to synthesize oxide nanoparticles has gained much attention in recent years. Chemical synthesis in a liquid phase through microwave irradiation for different duration and power involves heating of the material that takes place mostly because of dipolar polarization and ionic conduction mechanisms. Using this technique anatase TiO_2 nanoparticles have been synthesized [Ding et al. (2007); Dar et al. (2014)]

Microemulsion Technique

Microemulsions are considered as colloidal 'nano-dispersions' of water in oil or vice versa stabilized by a surfactant film. These dispersions are thermodynamically quite stable and can be regarded as nanoreactors that can be used to initiate chemical reactions for the synthesis of nanomaterials. Microemusion technique has been used to synthesize TiO_2 nanoparticles using titanium isopropoxide (TIP), polyoxyethylene tert-octylphenyl ether (TritonX-100), heptane and hexanol [Li et al. (2014)]

Combustion Technique

It deals with the gas-phase processing of material that offers minimum energy requirement, simple equipment and fast reaction using a sustainable exothermic solid-solid reaction among raw materials. In combustion synthesis, the adiabatic flame temperature due to exothermic heat exceeds the boiling point of the products. In this process, nanoparticles can be instantaneously formed as products due to gasification in the burning process and nucleation as

well as crystal growth in the cooling sublimation process. Using this technique anatase TiO_2 nanoparticles have been synthesized [Nagaveni et al. (2004)]

1.2.2 Synthesis of TiO_2 Nanowires/Nanotubes

Now-a-days, synthesis and application of TiO_2 based one dimensional semiconducting nanostructures have received remarkable attention for their scientific and technological aspects. After the discovery of TiO_2 nanotubes by Kasuga et al. (1998), extensive studies related to the growth and properties of TiO_2 based one dimensional nanostructure are being carried out. Different methods to grow nanowires such as templates, emulsions or polymeric systems, vapour transport methods, solution methods, electrochemistry etc. are reported in literatures [Zou et al. (2006)]. Besides these techniques, hydrothermal offers variety of microstrucyures to the product with simply varying the synthesis parameters like temperature, *p*H of precipitation, reagents/surfactants, reaction temperature, solvents etc. [Byrappa and Youshimura (2001)]. Basically, in hydrothermal technique/reaction the material is heated in the presence of autogenous pressure resulting from the heating beyond the boiling point of the aqueous solvent. This super-critical water exhibits special functions in facilitating the complex reactions, and results into unique structural features to the final product [Zou et al. (2006)]. However, in most of the cases, during the synthesis of TiO_2 nanowires, the phase changes to a meta-stable monoclinic TiO_2 (B) phase after hydrothermal treatment [Yoshida et al. (2005)] or a trace of brookite phase forms along with anatase phase [Zhang et al. (2002)]. Hydrothermal treatment with concentrated NaOH or KOH often changes the phase of the TiO_2 to undesirable Na_2TiO_6 or K_2TiO_6 respectively [Meng et al. (2006); Du et al. (2003)]. Synthesis of nanowires using sub-microscopic TiO_2 particles are also reported [Du et al. (2003)]. Regarding the mechanism of the nanowire/tube growth, reports suggest the formation of intermediate nanosheets due to hydrothermal treatment that roll up to form tubes after washing in dilute acid [Wang et al. (2002)]. However, Zhang et al. (2005) refutes the effect of washing procedure on the morphology of these

nanostructures. Hydrothermal reaction at high temperature often leads to the formation of nanowires instead of tubes [Armstrong et al. (2004)].

1.2.3 Deposition of Thin Films

Several techniques have been employed for the growth of thin films of TiO_2. These are pulsed laser deposition (PLD), metal organic vapour deposition (MOCVD), sputtering, molecular beam epitaxy (MBE), thermal evaporation, sol-gel, and e-beam evaporation. To deposit films, different substrates have been used like Si, Quartz, $LaAlO_3$, $SrTiO_3$, c-plane Al_2O_3 and glass. As the metastable anatase form of TiO_2 is difficult to produce in bulk, they can be fabricated in thin film form by choosing appropriate lattice-matched substrate. Films can be grown epitaxially on substrates with minimum lattice mismatch. Anatase TiO_2 has minimum lattice mismatch for $LaAlO_3$ substrates.

Pulsed Laser Deposition (PLD) Technique

It is the most versatile technique to deposit stoichiometric thin films by optimizing the different deposition parameters. It uses a pulsed laser beam to ablate the target material to deposit it on the substrate kept at a fixed temperature. The ablation process generates the plasma known as plume that is actually condenses on the substrate. There is an option to flow reactive gases like oxygen into the chamber during the deposition to compensate the oxygen loss. However, proper vacuum must be maintained for the plasma formation. TiO_2 and transition metal doped TiO_2 films of anatase and rutile phases have been grown using this technique [Yamamoto et al. (2001)].

Sputtering Technique

The word sputtering means to eject material from the target that ultimately gets deposited on the substrate to make a film. These sputtered ejected target atoms have a wide energy distribution. These atoms may ballistically fly from the target in straight lines and bombard on the substrates. There is a probable chance of re-sputtering in that case. To slow down these

ballistic sputtered atoms, some reactive gases are used. These gases make the sputtered atoms react and then they slowly gets deposited on the substrate. For sputtering, inert gas like Ar is preferred. However, for comparable momentum transfer, the atomic weight of the sputtering gas must be closer to the atomic weight of the target. Hence, for sputtering of light atoms, Ne is suitable whereas to evaporate heavy atoms Kr is preferable. The rate of motion of the sputtered particles can be controlled by changing the background pressure. The compounds having elements of different melting points are suitable for this method for deposition. TiO_2 as well as transition metal doped TiO_2 have been deposited by this technique [Zeman and Takabayashi (2002)].

Thermal Evaporation Technique

Thermal evaporation technique is based on the resistive heating process. It uses a resistance heating element in the form of a boat or coil to melt the material to raise its vapour pressure. The evaporation takes place in high vacuum. The material gets deposited in the gas phase on the selected substrate placed in front of the heater. Pressed pellet of TiO_2 powder material is mainly used as a target. In another way, thin films of Ti may be deposited on the substrates, and subsequent annealing in oxygen atmosphere may lead to the formation of phase pure TiO_2 films [Yadav et al. (2007)].

E-beam Evaporation Technique

In e-beam evaporation technique, the target material is placed inside a copper crucible that acts as an anode. An electron beam is bombarded from an electron gun on the material placed in the crucible. Upon striking the material, it evaporates and forms a gaseous phase that gets deposited on the desired substrates placed at a certain distance from the target. Besides the substrate, the material gets deposited inside the whole chamber. To prohibit this deposition on the electron gun, the beam of electron is bent through an obtuse angle by a magnet, so that it does not come in front of the target during deposition. TiO_2 thin films have been successfully deposited by this method [Yang et al.

(2004)]. In another way, Ti films can be deposited by this method, and then these films on oxidation yields TiO_2 [Chong et al. (2006)].

Sol-gel Spin Coating Method

Sol-gel spin coating is the most inexpensive method for thin film deposition. It does not require high vacuum or sophisticated machinery for the deposition. A liquid precursor prepared through sol-gel technique is used for deposition. The solvent is essentially volatile material that must evaporate after post-deposition annealing. A drop of solution is put on the substrate that is mounted on the spin coater by evacuation, is made to rotate by a motor with different rpm. In this way, the excess of the solution is removed from the substrate surface and a thin layer forms over it due to centrifugal force. The as deposited film necessarily be dried and annealed to achieve crystalline phase. By controlling the angular speed and solution concentration the thickness of the film can be controlled. Many layers can be formed by repeating the deposition and annealing process. Titanium isopropoxide or titanium butoxide dissolved in absolute ethanol is generally used for the deposition of TiO_2 thin films by spin coating technique [Ohya et al. (1996); Rath et al. (2009)]. For doping transition metals in TiO_2, corresponding metal acetates are dissolved in alcohol is mixed with the precursor solution before spin coating. The rpm and deposition time can be controlled through computer programs.

Molecular Beam Epitaxy (MBE) Technique

MBE is used to deposit high purity epitaxial thin films. This deposition technique is a form of sophisticated vacuum evaporation technique, in which directed neutral thermal atomic and molecular beams impinge on a heated substrate under ultra-high vacuum (UHV) conditions. For the creation of high vacuum, cryo-pumps are used. In this method films of uniform thickness (~ nm) can be grown [Joyce (1985)]. Undoped as well as doped TiO_2 thin films have been deposited by this method combining other techniques for the target evaporation process [Kim et al. (2004)].

MOCVD Technique

Metalorganic chemical vapour deposition (MOCVD), is basically a chemical vapour deposition technique commonly used to prepare single or polycrystalline thin films on different substrates. The deposition process is quite complex and is based on chemical reaction to achieve crystalline thin films. Instead of high vacuum requirements like MBE, the deposition can be done in the gas phase at moderate pressures. This technique has been used for preparing films for commercial optoelectronics devices. For the deposition of TiO_2 film, Ti based organometallic precursors are used [Won et al. (2001); Byun et al. (1997)].

1.3 Applications of TiO_2

TiO_2 is a potential semiconducting material that finds application in diverse fields. It is a well-known material for photocatalyisis [Linsebigler et al. (1995); Hashimoto et al. (2005)]. Due to its ability to degrade commercial dies under the UV irradiation, it has been studied for the waste water treatment [Li and Li (2001); Ruppert et al. (1994)]. It is commonly used as the white pigment in colours, paints, cosmetics and in the pharmaceutics industries [Morterra et al. (1992); Ayon (2006); Contado and Pagnoni (2008)]. It is non-toxic in nature and having antibacterial property that makes it applicable for the use as coatings [Yu et al. (2003)]. TiO_2 based polymer composites are now-a-days gaining much interest for different application point of view [Han et al. (2010); Pena et al. (1997)]. In particular, TiO_2 nanowires are important due to their potential application in dye sensitized solar cells (DSSC) [Paulose et al. (2006)], as an electrode for Li ion batteries [Armstrong et al. (2006)] and possible use in nano field effect transistors (FET) [Baik et al. (2008)]. TiO_2 is used as sensor for determination of chemical oxygen demand [Zheng et al. (2008)], gases like hydrogen [Mor et al. (2004)] and hydrogen sulphide [Lin et al. (1995)] and glucose [Bao et al. (2008)]. TiO_2 doped with transition metal exhibit room temperature ferromagnetism that makes it a possible oxide dilute

magnetic semiconductor (DMS) material. Before going to the details of oxide DMS, we present below a brief overview of the DMS materials.

1.4 Dilute Magnetic Semiconductors

Semiconductors doped with magnetic ions are being studied in an effort to develop spintronics, the new kind of electronics that seeks to exploit both charge and spin degrees of freedom [Zutic et al. (2004)]. The first so-called diluted magnetic semiconductors (DMS) were II-VI semiconductor alloys like $Zn_{1-x}Mn_xTe$ and $Cd_{1-x}MnTe$ originally studied in the 1980s [Furdyana (1988)]. These materials are either spin glasses or have very low ferromagnetic (FM) critical temperatures (T_C ~few K) [Ferrand et al. (2001)] and are, therefore, inadequate for technological applications which would require ferromagnetic order near room temperature. Further, Mn doped III-V semiconductors $In_{1-x}MnAs$ [Munekata et al. (1989); Ohno et al. (1992)] and $Ga_{1-x}MnAs$ [Ohno et. al. (1996); Jungwirth et al. (2006)] showed ferromagnetism at a much higher temperature due to the development of molecular beam epitaxy (MBE) growth techniques. The current high T_C record of 173 K is achieved in Mn-doped GaAs by using low temperature annealing techniques [Edmonds et al. (2002); Chiba et al. (2003)]. It is promising, but still too low for practical applications. For all these materials, ferromagnetism has been proven to be carrier mediated, a necessary property for spintronics since this enables the modification of magnetic behaviour through charge manipulation. This has motivated a quest for alternative spintronic materials with relatively higher T_C and carrier mediated ferromagnetism. In this direction, dilute magnetic semiconducting oxides [Janisch et al. (2005)], such as transition metal doped TiO_2 [Matsumoto et al. (2001)], ZnO [Ueda et al. (2001)], and SnO_2 [Ogale et al. (2003)], could represent the alternative with T_C s above room temperature and as high as ~ 700K [Shinde et al. (2003)]. Among the oxide DMS materials, we focus only on the TiO_2 based DMS.

1.4.1 TiO_2 Based DMS

Room temperature ferromagnetism was first discovered in Co (~7 at %) doped TiO_2 by Matsumato et al. (2001) followed by Chambers et al. (2001). Later lots of research work emerged to demonstrate ferromagnetism in these systems by different deposition techniques as mentioned earlier. The obtained results indicate strong dependence of growth parameters on the structural, electrical and magnetic properties. Magnetic properties of the doped TiO_2 critically depend on the dopants solubility in TiO_2 matrix. Above some critical value, the dopant starts agglomerating as impurity. However, the magnetic moment for the same dopant concentration is also not achieved by different techniques. For example in case of 7 at.% Co doped TiO_2 the magnitude of saturation magnetisation ranges from 0.32 to 1.7μ_B. It suggests the growth parameters like substrate, oxygen partial pressure, deposition temperature and phase of TiO_2 determines the solubility of dopant in host matrix showing the ferromagnetic order. However, the results are always not reproducible and often criticized for the possible role of contamination giving rise to the observed magnetism. Besides Co several cations like V, Cr, Fe, Ni and Cu have been doped in TiO_2 to study the observed magnetism. After the discovery of ferromagnetism in undoped TiO_2, the probable role of dopants inducing the magnetic order becomes controversial. Whether transition metal dopants or oxygen vacancies are the possible source of magnetism is still not established. There are several proposed mechanisms in literature that explains the possible ferromagnetism in DMS materials. However, no single model could explain the observed ferromagnetism completely. The literatures on various doping in TiO_2 are given in Chapter II.

1.4.2 Possible Origins of Ferromagnetism in DMS

In this section, we discuss different mechanisms in terms of interaction of spins proposed for the origin of magnetism in diluted magnetic semiconductors. For example, double exchange interaction that leads to ferromagnetism whereas the other mechanisms lead to either ferromagnetic or antiferromagnetic interactions depending on the nature of the bonding, structure, type of defect , and/or carrier concentration.

Exchange Interaction in Insulators: direct and superexchange

(a) Direct exchange

Magnetic exchange interactions are usually written in the form of a spin hamiltonian as

$$\mathscr{H}_{ij} = -\sum J_{ij} \mathbf{S}_i . \mathbf{S}_j \quad \text{.....(1.5)}$$

The parameter $\mathscr{H}_{ij}$ couples the spin at lattice sites *i* and *j*. Direct exchange involves an overlap of electronic wave functions from the two sites and the Coulomb electrostatic repulsion. The Pauli's exclusion principle makes the electrons with parallel spin away from each other, to reduce the Coulomb repulsion. The difference in energy for parallel and antiparallel configurations is known as the exchange energy. Basically, an antiparallel configuration is preferred as the simplest case of the hydrogen molecule. Since the wave functions of the magnetic '*d*' or '*f*' electrons decrease exponentially with distance from the nucleus, the J_{ij} obtained from the overlap integral is quite small to provide the necessary coupling. If the interaction takes place between localized electrons on different neighbouring atoms, J_{ij} tends to be negative corresponding to a situation where two electrons align antiparallel to form a bonding state. In a solid having unpaired number of electrons, the sign of J_{ij} in principle be either positive or negative, but in most of the cases negative part dominates leading to antiferromagnetic alignment of the neighbouring spins [Mydosh (1993); Janisch et al. (2005)].

(b) Superexchange

In case of transition metal oxides and related materials, magnetic interactions between the transition metal ions are mediated by the intermediated anions leading to a Superexchange interaction. Superexchange interaction can be described by a Heisenberg Hamiltonian, where the sign of J_{ij} is determined by the metal-oxygen-metal bond angle and the *d* electron configuration on the transition metal. The corresponding results are summarized in the compendium of work based on the semi-empirical Goodenough-Kanamori-Anderson rules [Janisch et al. (2005)].

Carrier mediated exchange interaction (RKKY, Zener carrier mediated exchange and Zener double exchange)

The phrase 'carrier-mediated exchange' typically refers to the interactions among the localized moments that are mediated by free carriers in the system. Below we emphasize on three limiting cases: the RKKY interaction, Zener carrier mediated exchange and Zener double exchange interaction. In most of the cases, the system exhibit features of two or all of the modes [Janisch et al. (2005)].

RKKY: For the magnetic alloys, the conduction electrons lead to stronger and long-range indirect exchange interaction. This is the now famous Ruderman-Kittel-Kasuya-Yosida (RKKY) interaction whose Hamiltonian is $\mathscr{H} = J(\mathrm{r})\mathbf{S}_i \cdot \mathbf{S}_j$. Embedding the magnetic impurity, i.e., a local moment (spin $\mathbf{S}_i$), in a sea of conduction electrons with itinerant spin $\mathbf{s}(\mathbf{r})$ causes a damped oscillation in the susceptibility of the conduction electrons, and thereby a coupling between spins ($\mathbf{S}_i$ and $\mathbf{S}_j$) following the relation

$$J(r) = 6\pi Z J^2 N(E_F) \left[\frac{sin(2k_F r)}{(2k_F r)^4} - \frac{cos(2k_F r)}{(2k_F r)^3} \right] \ldots\ldots\ldots\ldots\ldots\ldots (1.6)$$

where Z is the number of conduction electrons per atom, *J* is the *s-d* exchange constant, $N(E_F)$ is the density of states at the Fermi level, k_F is the Fermi

momentum and r is the distance between two impurities. The above expression reduces to

$$J(r) = \frac{J_0 cos(2k_F r + \phi)}{(2k_F r)^3} \ldots\ldots\ldots\ldots\ldots\ldots\ldots\ldots\ldots\ldots\ldots\ldots (1.7)$$

for large distance. A phase factor ϕ has been introduced to account for the charge difference between impurity and host and the former's angular momentum [Mydosh (1993)].

Zener carrier mediated exchange: Systems having both local magnetic moments and itinerant carriers (doped DMS) where the carriers can possibly mediate a ferromagnetic interaction among the local magnetic moments is termed as Zener carrier-mediated exchange [Zener (1951a); Zener (1951b)]. The ferromagnetic ordering is established by lowering of the carrier's energy due to redistribution between spin subbands split apart by the exchange interaction [Janisch et al. (2005)].

Zener double-exchange: It has been proposed to explain the observed magnetism in doped perovskite structure manganites, $La_{1-x}A_xMnO_3$, with A = Ca, Sr, or Ba. For intermediate values of $0 < x < 1$ both Mn^{4+} (with three 3d electrons) and Mn^{3+} (with four 3d electrons) are present. If the magnetic ions align parallel, the kinetic energy of the system is lowered leading to electron transfer from Mn^{3+} to Mn^{4+}. This type of coupling is accompanied by oxygen atoms between neighbouring Mn^{3+} and Mn^{4+} ions, but is different from the superexchange by the involvement of the carriers [Zener (1951c)].

Bound Magnetic Polarons (BMP)

In the BMP model, oxygen vacancies act as electron donors as well as traps electron that can hold the electrons and maintain insulating behaviour. Every trapped electron couples the local moments of the host lattice that lie within its orbit ferromagnetically, forming a bound polaron with a net magnetic moment. In case of two neighbouring polarons don't couple strongly, a

paramagnetic insulating phase forms. Though, for certain polaron-polaron distances and combinations of electron-electron and electron-local moment exchange constants, the polarons may interact in a ferromagnetic sense [Drust et al. (2002); Angelescu and Bhatt (2002)]. In general, the critical distance above which the exchange between two BMPs becomes ferromagnetic is of the order of a few Bohr radii [Angelescu and Bhatt (2002)]. The amplitude of the exchange interaction further decreases rapidly with distance. Beyond some critical electron density, the attractive potential related to the vacancy is screened, as a result, the donor electrons become free making the system metallic (analogously to a Mott insulator-metal transition) [Kübler and Vigren (1975)]. Temperature also affects the formation/interaction of such BMPs. If there are sufficiently large numbers of polarons, they can give rise to net global ferromagnetic order in the system. The schematic picture of this interaction is given in Fig.1.3. This model is widely used to explain the ferromagnetism in insulating oxide DMS.

Charge-transfer or Stoner Ferromagnetism

This type of magnetism was first proposed by Coey et al. (2008) in oxide nanoparticles. In case of magnetic impurities distributed randomly in the oxide materials; isolated ions, pairs and clusters will form at dopant concentrations '*x*' below percolation limit (Fig.1.4 (a)). The cations that couple through an oxygen ligand is superexchange (i.e. antiferromagnetic) leading to a Curie-Weiss behaviour in susceptibility whereas isolated ions and small clusters demonstrate Curie-like behaviour (Fig.1.4 (b)) [Coey et al. (2008)].

In case of insulating or nonmetallic systems, RKKY mechanism is seized. Electron transfer to the defect states in the nanoparticle could enhance the Fermi level (E_F) to a peak in the local density of states where the Stoner criterion for magnetism may be satisfied. This criterion is given as:

$$N(E_F) > 1/I$$

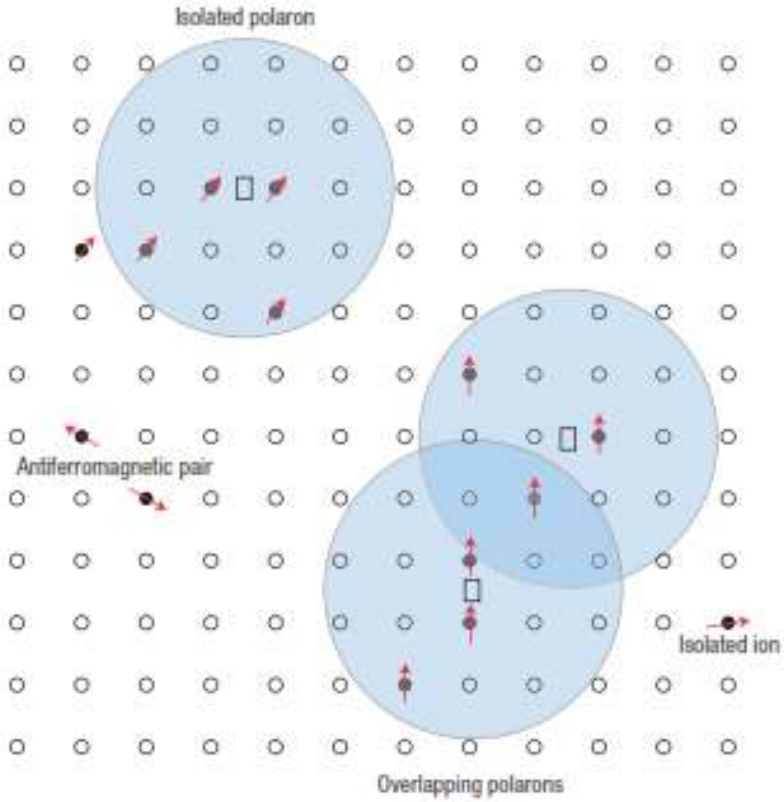

Fig.1.3 A donor electron in its hydrogenic orbit couples with its spin antiparallel to impurities with a 3d shell that is half-full or more than half-full. Cation sites are represented by small circles. Oxygen is not shown; the unoccupied oxygen sites are represented by squares. [After Coey et al. (2005)]

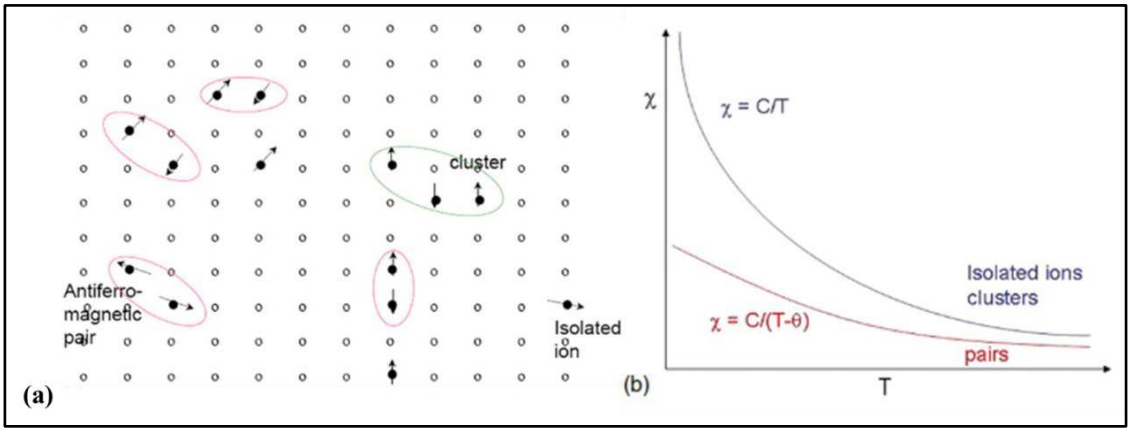

Fig.1.4 Schematic illustration of (a) the distribution of magnetic cations in a dilute magnetic oxide and (b) the resulting magnetic susceptibility. [After Coey et al. (2008)]

where N(E) is the density of states at the Fermi level and I is the Stoner parameter (~1 eV). This model is based on the spin-split band theory instead of Heisenberg exchange coupling of localized spins. In this mechanism, moments of the transition-metal dopant cations do not play the essential role. The prime requirement is that the transition metal atom should have multiple valence states. Also, the ferromagnetism is completely nonuniform throughout the samples and only restricted to some defect-rich regions like the surface of the oxide nanoparticles.

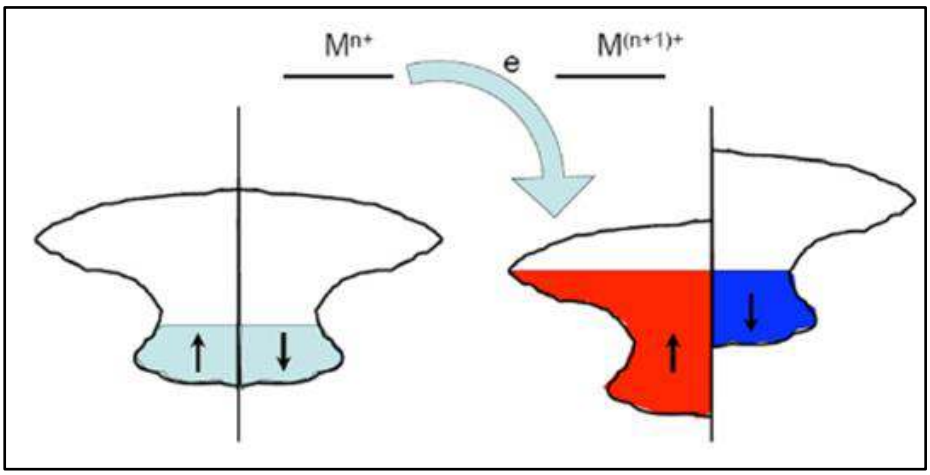

Fig.1.5 The charge transfer involved in a system with a ferromagnetic instability. [After Coey et al. (2008)]

The 3*d* dopants behave like a charge reservoir from which electrons are transferred to local defect states exist at or near the particle surface. The principle of charge-transfer ferromagnetism is shown in Fig.1.5. In this mechanism, the magnetism of the dopant is insignificant. However, these cations may contribute to the observed magnetism; their ability to feed electrons locally into the conduction band (or accept charge from it) that explains the dopant cation's ability to favour ferromagnetism is of main importance. However, detailed experiments as well as theoretical calculations are necessary to validate the conjecture.

1.5 Material Modification by Ion Matter Interaction

Interaction of energetic charged particles on solid target leads to ion penetration, rearrangement of target atoms, excitation of electrons and emission of particles and other forms of radiation from the surface. When energetic ion penetrates a material, it loses energy mainly by two nearly independent processes: (i) elastic collisions with the nuclei known as nuclear energy loss $(dE/dx)_n$ or S_n, and (ii) inelastic collisions of the highly charged projectile ion with the atomic electrons of the matter known as electronic energy loss $(dE/dx)_e$ or S_e. In the inelastic collision (cross-section ~10^{-16} cm^2) the energy is transferred from the projectile to the atoms through excitation and ionization of the surrounding electrons. The amount of electronic energy loss in each collision varies from tens of eV to a few keV per Angstrom (Å).

The energy deposited on the material is commonly described by the linear stopping power $S = S_e + S_n$, that indicates the energy deposited or transferred per path length of an incident particle along its trajectory. It is also known as specific energy loss. The path travelled by the projectile ion through the matter is called the projected range (R_p). It is numerically defined as the integral of the reciprocal of the stopping power integrated over the total energy loss as represented by equation (1.8):

$$R_T = \int_0^{E_0} \frac{dE}{\left(\left(\frac{dE}{dX}\right)_e + \left(\frac{dE}{dX}\right)_n\right)} \dots\dots\dots\dots\dots\dots\dots (1.8)$$

In a practical sense, the stopping power indicates the strength of the target material to slow down and stop an incident projectile ion. Nuclear stopping power (S_n) dominates at the projectile energy of around 1keV/amu and the projectile ion is called "low energy ion" where the projectile ion transfers its momentum to the target atoms via elastic interaction processes. In case of electronic stopping power (S_e), it dominates in the energy regime of 1MeV/amu or more and the projectile is known as 'Swift Heavy Ion' and is abbreviated as SHI. Here the interaction of projectile and target takes place via inelastic process. Both S_e and S_n increases with energy till they reach a maximum value and decreases thereafter. A typical behaviour of S_e and S_n is

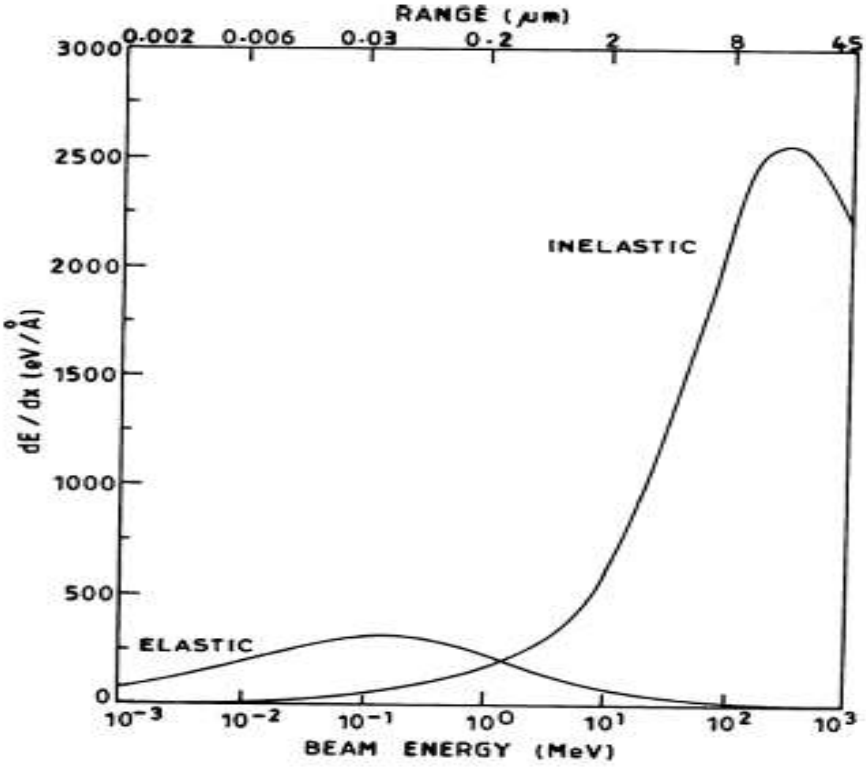

Fig.1.6 Curves showing the variation of electronic and nuclear energy loss corresponding to the inelastic and elastic collisions respectively of silver beam passing though YBCO at various energies. [After Kanjilal (1997)]

shown as Fig.1.6. The S_e reaches its peak value that is orders of magnitude higher than the peak energy corresponding to S_n. Swift heavy ions moving through the solid lose most of its energy through electronic excitations and ionization of the target atoms except at the end of the trajectories where elastic nuclear collisions dominates.

A swift heavy ion (SHI) moving at a velocity comparable to the Bohr velocity of the electron transfers the energy to the material and produces tracks when its value crosses a threshold value. The diameter and length of the track depend on the type, energy of the ion beam, electrical and thermal conductivity of the material. The interaction of SHIs with target material is quite different and unique compared to energetic photon or electron irradiation. SHI may deposit huge amount of energy in a highly localized region (~10^{-17} to 10^{-16} cm^3)

within a very short interval of time (~10^{-17} to 10^{-15} s) [Fink and Chadderton (2005)]. The low or high energy ion interaction with solid leaves some modification in the material as a foot mark.

1.5.1 Material Modifications Due to Nuclear Energy Loss (S_n)

In the low energy regime (keV ions), the nuclear energy loss is the dominant process for losing energy of the projectile atom in a material medium and consequently leads the system to a non-equilibrium and excited state. The relaxation of the excited states can induce various types of defects in the material. The material modification takes place directly from keV ion bombardment that results: (i) ion implantation, which can lead to the accumulation of a concentration profile of foreign atoms within a solid, thus altering composition. The distribution of foreign atoms depends on the ion energy and the stopping processes that determine how individual ions slow down and upto what depth can they penetrate; (ii) atomic displacement from their regular lattice sites due to elastic collision; (iii) displacement of cascade of atom; (iv) atomic mixing at a temperature where normal diffusion processes would not operate. [Dearnaley et al. (1973)].

1.5.2 Material Modifications Due to Electronic Energy Loss (S_e)

The electronic energy loss and the consequent material modifications is much complex as compared to nuclear energy loss. It leads to coherent excitation of electrons along the ion path. The consequent modifications are the creation of amorphous latent track regions along the ion path when the $S_e > S_{eth}$. The threshold value of electronic energy loss (S_{eth}) is completely material dependent. It is different for different materials. If S_e is less than S_{eth}, some additional defects may appear [Dunlop et al. (1990)] and some times, the pre-existing defects can anneal out [Iwase et al. (1987)]. It can also induce structural phase transition around the ion path [Roller and Bolse (2007)]. In amorphous materials, the SHI irradiation can cause a macroscopic flow of matter [Klaumünzer and Schumacher (1983)]. The dimension of the amorphous latent tracks, which depends on both S_e and on the target material, varies from a

few nanometers in diameter and several micrometers in length. The diameter to length aspect ratio of the amorphous latent tracks is about 1:1000. The diameter of the ion track generally scales with the electronic energy loss for a material. More is the energy loss more will be the diameter. For the same electronic energy loss of two different ions having different energy, an interesting effect has been observed. The effect goes by the name "velocity effect". Here one find more the velocity, less is the track diameter. This velocity effect has been theoretically predicted by Katz and Kobetich (1969) and by Waligorski el al. (1986). These predictions have been validated by many authors [Meftah et al. (1993); Costantini et al. (1992)].

Though the application of sophisticated characterisation methods like high resolution transmission microscopy (HRTEM), near field microscopy, defect spectroscopy and x-ray diffraction resulted in a significant progress in collecting experimental data about track formation and track structures in solids, the mechanisms by which the electronic excitation energy is converted into atomic motion and finally to stable structural changes have no direct experimental technique to observe. This is due to the extremely short time scales (~ picoseconds) involved in the dynamics of structural modification. But these can be described by various models invoked over the years. These models relate to such phenomena as localisation of kinetic energy, formation of positive charge core followed by coulomb explosion and/or thermalisation and localised melting [De La Rubia et al. (1987); Itoh et al. (2009)]. Thus, there are two competing processes outlined in the literature. One is known as the Coulomb explosion model [Fleischer et al. (1965)], and the other is the thermal spike model [Wang et al. (1994)]. Brief overviews of these models are discussed in the next segment.

1.5.3 Coulomb Explosion Model

The Coulomb explosion model envisages that the SHI passing through the medium in a time scale ~ 10^{-17} sec with velocity of ~ 1 cm/nano-sec partially strips the material of electrons along its path. The time to cover atomic

sites by the projectile is short in comparison to the response time of the conduction electrons to neutralize it. So during the passage of the ion, a long cylinder containing positive charged ions is produced. This cylinder containing the charged ions explodes radially due to Coulomb's repulsion and hence creates an amorphous latent tack. This model is highly successful for explaining track creation in insulators where electrical neutrality along the ion path cannot be restored due to unavailability of mobile electrons. Later it is found that tracks can also be created in some metals like Bi, Fe, Ni, Ti at very high value of S_e (S_e > 40 keV/nm) [Fleischer et al. (1965); Dammak et al. (1993); Henry et al. (1992)].

1.5.4 Thermal Spike Model

The other competing process is the thermal spike model, which drives the excited electrons along the ion path and equilibrates to define a temperature called the electronic temperature in a time scale ~ 10^{-15} sec. These hot electrons then transfer their energy to the lattice through electron-phonon coupling so that the lattice heats up along the narrow cylindrical zone to attain its maximum temperature in a time ~ 10^{-14}-10^{-12} sec. If the lattice temperature exceeds its melting temperature, then the lattice melts in the confined narrow cylindrical zone. At a later time ~ 10^{-9} sec, the melted lattice delivers its energy to the surrounding medium at extremely high rate. That is, the lattice quenches with a quenching rate ~ 10^{15} K/sec leading to an amorphous column along the ion path. This model thus predicts the formation of ion tracks of a few nanometer diameter and of micron size length in a time scale ranging from a few picoseconds to a about nanosecond. As the time scale for the ion matter interaction is very short, it is physically very difficult to record the changes during the irradiation process. Only the changes retained after the irradiation process is studied ex-situ [Wang et al. (1994)].